Journal of Structural Geology, Vol. 12, No. 3, pp. 375 to 381, 1990
Printed in Great Britain

0191-8141/90 $03.00+0.00

Finite difference modelling of sandbox analogues, compaction and detachment free deformation

DAVID WALTHAM

Department of Geology, Royal Holloway and Bedford New College, University of London, Egham Hill, Egham, Surrey TW20 0EX, U.K.

(*Received* 29 *June* 1989; *accepted in revised form* 9 *October* 1989)

Abstract—The finite difference method, for the modelling of hangingwall deformation above faults, is applied to a wider range of problems. Close agreement has been achieved with the overall geometry of hangingwalls in sandbox analogue models of extensional faulting. These results give insights into the dynamics involved and zones of faulting can be indicated using stretch rate and shear rate maps. The controlling equations are then presented in a more general form which allows the effects of compaction to be included. Finally, the method is shown to be applicable to vertical and horizontal velocities (rather than speed and direction) and this has been used to model the crust deforming by brittle failure at the top, pure shear at the bottom and with a brittle–ductile transition in between. This system therefore allows modelling of crustal extension without the use of a detachment.

INTRODUCTION

THIS paper extends the methods introduced by Waltham (1989) in which the mathematics for using finite difference techniques was presented. The underlying idea of this approach is that deformation may be considered in terms of the velocity of movement at each point in the hangingwall. Given this velocity field, the hangingwall geometry can be computed as it evolves during extension (or compression). The choice of possible velocity fields is restricted by requiring that no compaction occurs and this gives rise to one equation at each point in the hangingwall. However, there are two unknowns (horizontal and vertical velocity or, alternatively, speed and direction) and one of these must therefore be supplied. In Waltham (1989) this was tackled by requiring that particle displacement directions be specified throughout the hangingwall. The particle displacement rates were then calculated using this supplied direction field. Thus, a new geometric method for forward modelling of hangingwall geometry, given a bounding fault and amount of extension, was presented. This method is superior to previous approaches (see Williams & Vann 1987, for an excellent review) in that it does not require simplifying assumptions such as vertical simple shear (Verrall 1982) or inclined simple shear (White *et al.* 1986) although these can be modelled as special cases. However, as a direct result of the finite difference method's increased generality, inverse modelling to predict fault geometry from hangingwall deformation is not usually possible and the method of White *et al.* (1986) is preferable for tackling this particular problem.

In this paper, finite difference techniques are extended to investigate a larger variety of problems. My intention is to present extensions to the method of Waltham (1989) although some interesting results incidentally emerge from the examples I use. I examine four new aspects of finite difference modelling. These are:

(1) the problem of simulating sandbox analogue models is investigated and it is shown that the geometry of a numerically modelled hangingwall can be made to approximate closely that of the equivalent analogue model;

(2) faulting within the hangingwall is clearly an important process in accommodating deformation and this is difficult to simulate since the finite difference approach deals best with quantities which vary smoothly with position. An indication of the likely positions of heavily faulted regions may be obtained by calculating stretch rate and shear rate maps from the velocity field used to generate the numerical result;

(3) the finite difference technique is extended to allow for sediment compaction during burial. An example is given which shows the effect of this on deformation during extension above a listric detachment;

(4) finite difference simulations can be performed using vertical and horizontal velocities rather than speed and direction. Many problems are more easily solved using this Cartesian approach. An example is given in which extension is accommodated by brittle failure in the top of a model and a uniformly distributed stretch at the bottom. The central portion of the model therefore represents a brittle–ductile transition zone. An important feature of this model is that it models crustal extension without using a detachment to decouple brittle failure in the upper crust from a ductile lower crust.

SIMULATION OF ANALOGUE MODELLING RESULTS

Hangingwall deformation may be simulated using sandbox analogue modelling methods (Cloos 1968, Faugere & Brun 1984, McClay & Ellis 1987). In McClay & Ellis (1987) deformation was simulated by progressively deforming layers of sand held between glass sidewalls.

The deformation was achieved by building the sand layers upon a plastic sheet and then slowly pulling this sheet along a predefined detachment surface. Thus, the displacement rate was constant along the entire fault surface including the detachment and curved listric part of the fault. In terms of computer modelling, this is a different boundary condition to that employed in Waltham (1989). Note that, with a constant displacement rate along the fault, deformation cannot be described in terms of simple shear along inclined planes since this requires that the component of velocity perpendicular to the shear planes is constant (White *et al.* 1986). In other words, inclined (or vertical) shear models will produce different displacement rates at different parts of a curved fault.

Extensive comparisons of the results from analogue and computer models have been carried out in order to confirm that the computer models have the right general behaviour and as an aid in understanding how the analogue models have deformed in terms of displacement rates and displacement directions of individual particles. A single example is shown here to illustrate the method.

Figure 1(a) shows an interpretation of a 26 cm long analogue model after extension by an additional 26 cm above a listric detachment. The alternating black and white layers represent pre-rift sediments whereas the unshaded layers are syn-rift. Syn-rift layer boundaries have been introduced after each 1 cm increment of extension. The general geometry shown in Fig. 1(a) is typical of those produced in analogue model runs with listric bounding faults. Figure 1(b) is the corresponding computer model with a grid representing the pre-rift sediments and simple layers representing the syn-rift sediments. The syn-rift boundaries in the computer model have been introduced after each 2 cm of extension. The displacement direction contours at 5° intervals are shown in Fig. 1(c) and these were chosen by a process of trial and error to produce a reasonable match between the numerical and analogue models. The contour values equal the fault dip at the fault–contour intersections.

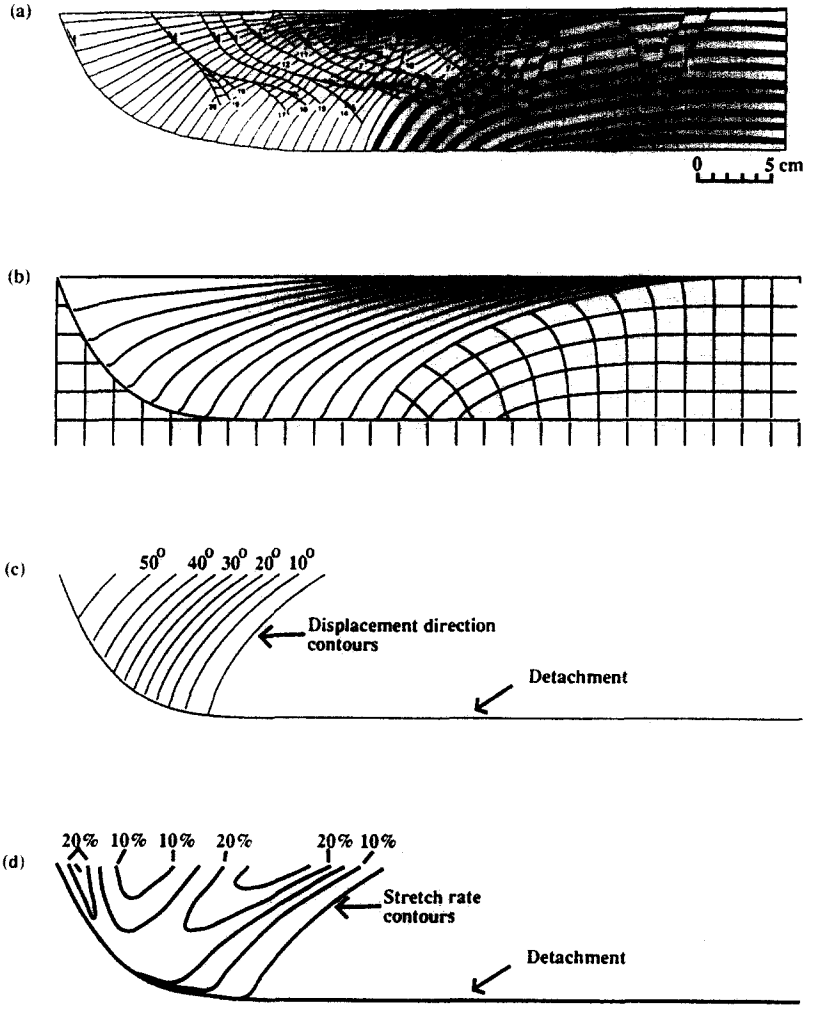

Fig. 1. Computer simulation of a sandbox analogue model. The model was initially 26 cm long and has been extended by an additional 26 cm. (a) Interpretation of sandbox result, black/white layers are pre-rift and plane layers are syn-rift. (b) Corresponding finite difference model, grid represents pre-rift sediment and simple layers are syn-rift. (c) Displacement direction contours at 5° intervals with contour value equal to fault dip at contour–fault intersection. (d) Hand contoured stretch rate map. Contour values are as a percentage of the maximum value.

Ignoring for the moment the effects of small-scale internal faulting, the overall geometries of the two models are similar with a very steep pre-rift–syn-rift boundary near the detachment and high curvature of this boundary at 2–3 cm above the detachment. In both models, this boundary becomes much less steep towards the right of the figure. This geometry is impossible to achieve with inclined simple shear since a steep shear plane dip would be required near the fault to get a high curvature on the pre-rift–syn-rift boundary whereas a shallow dip would be needed at the top of the model to achieve a broad enough region of deformation. In Waltham (1989) it was demonstrated that the direction contours are related to the shearing surfaces and in Fig. 1 these contours are subparallel to the final positions of the bedding planes. This implies that a large amount of deformation has occurred by slippage between beds, a conclusion which could not easily be reached by any other method.

SHEAR AND STRETCH RATES

Strain, both in real hangingwalls and the analogue models discussed above, is usually localized rather than uniformly distributed, resulting in brittle faulting. Thus, to relate the deformation produced in the finite difference modelling to the observed faulting of real cases, it is necessary to investigate how strain varies within the hangingwall. Shear strain and extension strain are easily calculated from the velocity field.

Equations relating strain (or strain rates) to displacement (or displacement rates) are well known (e.g. Jaeger 1956). For extension rate, $\dot{\varepsilon}$, the expression is

$$\dot{\varepsilon} = (\partial v_x/\partial x)\cos^2\alpha + (\partial v_x/\partial z + \partial v_z/\partial x)\sin\alpha\cos\alpha + (\partial v_z/\partial z)\sin^2\alpha. \quad (1)$$

The directions of maximum extension rate (the stretch rate) and the minimum extension rate are given by the two solutions of

$$\tan 2\alpha = (\partial v_x/\partial z + \partial v_z/\partial x)/(\partial v_x/\partial x - \partial v_z/\partial z). \quad (2)$$

Similarly, the shear rate, $\dot{\gamma}$, is given by

$$\dot{\gamma} = (\partial v_z/\partial z - \partial v_x/\partial x)\sin 2\alpha + (\partial v_x/\partial z + \partial v_z/\partial x)\cos 2\alpha. \quad (3)$$

Thus, using equations (1)–(3), the stretch rate and shear rate at each point in the hangingwall can be calculated from the velocity field found using the finite difference method. Figure 1(d) shows the stretch rate for the example used in the previous section. This stretch rate is displayed using contours with an increment of 5% of the maximum stretch rate. The maximum stretch rate (0.35 of the extension rate) occurs near the top of the steep part of the bounding fault. These high rates near the fault indicate that slippage is occurring between the sand and the plastic detachment sheet and this slippage is indeed observed in the analogue model. The region of high strain in the hangingwall compare reasonably well to the position of early faulting found in the analogue model (faults 1 and 2 in Fig. 1a). It must be remembered, when comparing Figs. 1(d) and (a), that the faults have been transported away from their positions of formation by subsequent extension.

MODELLING COMPACTION

The assumption has been made, up to this point, that the material undergoing deformation is incompressible. However, real sediments undergo compaction as they are buried. The finite difference technique should include compaction and a minor modification to the method allows it to do so.

The starting point is conservation of mass which, for a flowing medium, requires that the equation of continuity

$$\nabla\cdot(\rho\mathbf{v}) + \partial\rho/\partial t = 0 \quad (4)$$

(Birkhoff 1955) is satisfied. Here, ρ is matrix density, v is vector velocity and t is time. This expresses, mathematically, the idea that if material flows into a fixed volume at a rate which is different to that at which it flows out (this difference is expressed by the first term in equation 4) then the density within the volume must alter (the rate of change of density is given by the second term).

I now make the assumption that the material is homogeneous, apart from a depth-dependent density variation. In other words, I assume that density variations are the result of burial alone. The second term in the above equation becomes zero and the first term can be rearranged to yield

$$\nabla\cdot\mathbf{v} + (v_z/\rho)(\partial\rho/\partial z) = 0, \quad (5)$$

where v_z is the component of velocity in the vertical, z, direction. Note that, if density does not alter with depth, equation (5) reduces to $\nabla\cdot\mathbf{v} = 0$ which was the fundamental equation used in Waltham (1989). Transforming equation (5) from horizontal and vertical components of velocity (v_x and v_z) to speed, v, and direction, θ, using

$$v_x = v\cos\theta \quad (6)$$
$$v_z = v\sin\theta \quad (7)$$

leads to

$$\partial v/\partial x + (\partial v/\partial z)\tan\theta = v((\partial\theta/\partial x)\tan\theta - \partial\theta/\partial z - (\tan\theta/\rho)(\partial\rho/\partial z)) \quad (8)$$

which may be solved using the method of Waltham (1989).

The density variation, $\rho(z)$, can have any reasonably smooth form (i.e. it should be well sampled at the finite difference grid interval). One example arises from assuming exponential decay of porosity, ϕ, with depth (Magara 1978, Steckler & Watts 1978, Sclater and Christie 1980), i.e.

$$\phi = \phi_0 e^{-z/\lambda}, \quad (9)$$

where ϕ_0 is the porosity at surface and λ is the depth at which porosity has been reduced to ϕ_0/e. For a matrix

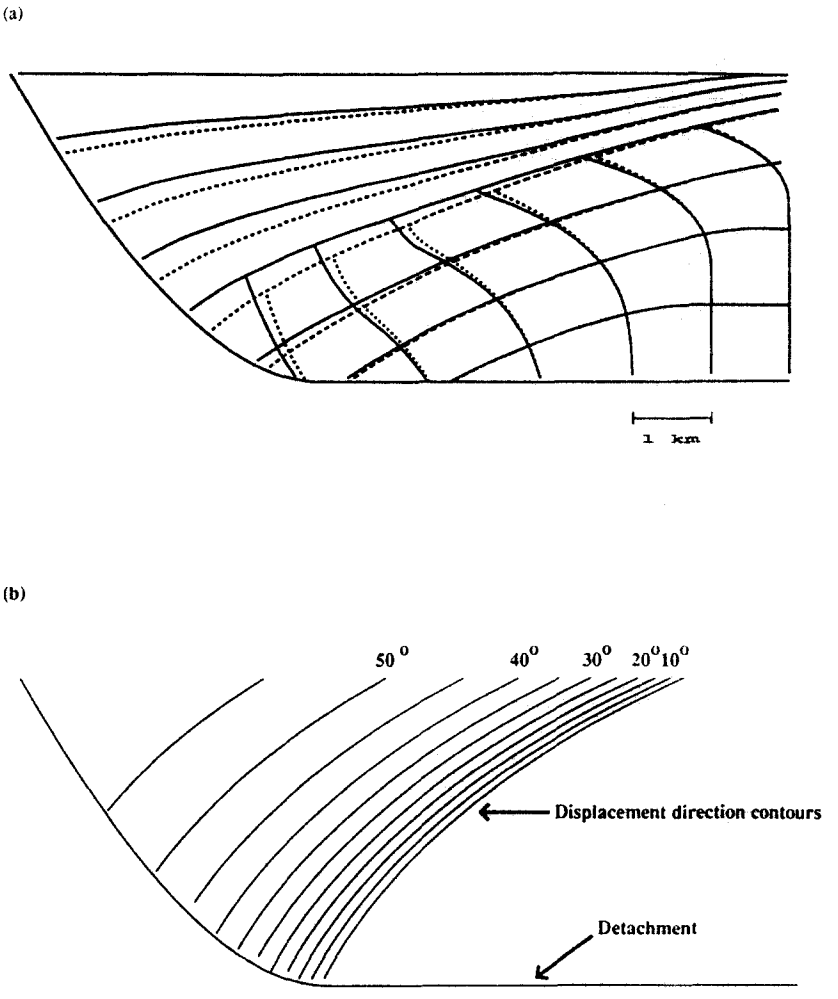

Fig. 2. The effect of compaction on deformation during extension by 4 km above a listric detachment. The porosity at the surface was 40% falling exponentially to 15% at a depth of 2 km. The matrix density was 3 Mg m^{-3}. (a) Solid lines represent the result for no compaction and the dotted lines represent the result with compaction. The grids show the geometry of the pre-rift material and the curved lines show the syn-rift material. (b) Displacement direction contours at 5° intervals with contour value equal to fault dip at contour–fault intersection.

with compacted density ρ_m this produces a depth-dependent density of

$$\rho = \rho_m(1 - \phi) \tag{10}$$

from which it follows that

$$\partial\rho/\partial z = \rho_m\phi/\lambda. \tag{11}$$

An example which uses these expressions is now given.

Figure 2 illustrates the effect of compaction on hangingwall geometry above a listric fault with a detachment depth of 4 km. Note that the zero-gradient boundary conditions of Waltham (1989) have been used in this example rather than the constant-speed boundary condition discussed in the previous sections. An extension of 4 km has been used together with the displacement direction contours shown in Fig. 2(b) (5° contour interval). In Fig. 2(a) the zero compaction result is shown with a full line whereas the result which includes compaction is shown with a dashed line. The parameters used were $\phi_0 = 40\%$, $\rho_m = 3$ Mg m^{-3} and $\lambda = 2000$ m. Pre-rift sediments are represented by the initially square 1 km grid and syn-rift sediments have been simulated by introducing a horizontal line at surface after every 500 m of extension. The difference between the two results is most noticeable in the top layer of the pre-rift sediments which thins from right to left in the compacted result compared to the non-compacted result. Note that compaction has produced increased subsidence of the hangingwall with a greater thickness of syn-rift sediment and a slightly accentuated rollover. The deeper pre-rift sediments are not greatly affected since they do not undergo a large change in burial depth and were, in any case, already significantly compacted.

Interesting comparisons can be made between Fig. 2(a) and the results shown in White *et al.* (1986). Both sets of results show a compaction effect which increases with depth for syn-rift sediments but decreases with depth for the pre-rift sediments. However, there the similarity ends. The results of White *et al.* (1986) show a hangingwall syncline produced by differential compaction whereas this is not seen in Fig. 2(a). This compaction syncline results from the assumption of uniaxial compaction parallel to the inclined shear planes which necessarily prevents compaction from altering bed positions on the bounding fault. However, no such uniaxial compaction assumption has been made in the derivation

of equation (8) and so compaction in a direction parallel to the bounding fault is permitted. Thus, a hangingwall syncline is not a *necessary* geometric consequence of compaction although it may yet be shown that it is a physical consequence of compaction.

MODELLING A BRITTLE–DUCTILE TRANSITION

Figure 3 illustrates the application of the finite difference method to a brittle–ductile transition problem. The model has undergone 5% extension with brittle failure in the top third, ductile behaviour in the bottom third and with transitional behaviour in the central third. As before, the pre-rift material is represented by an initially square grid and the syn-rift geometry is illustrated by simple layering. Figures 3(b) & (c) model slightly different behaviour in the plastic region.

This diagram has been produced by calculating vertical velocity from horizontal velocity rather than by finding displacement rate from the displacement direction. For many problems the solution is more easily found using this Cartesian framework. The general approach is to specify horizontal velocity everywhere together with the vertical velocity on the bottom, left and right boundaries. The vertical velocity field within the block is then calculated using

$$\partial v_z/\partial z + \partial v_x/\partial x = 0. \quad (12)$$

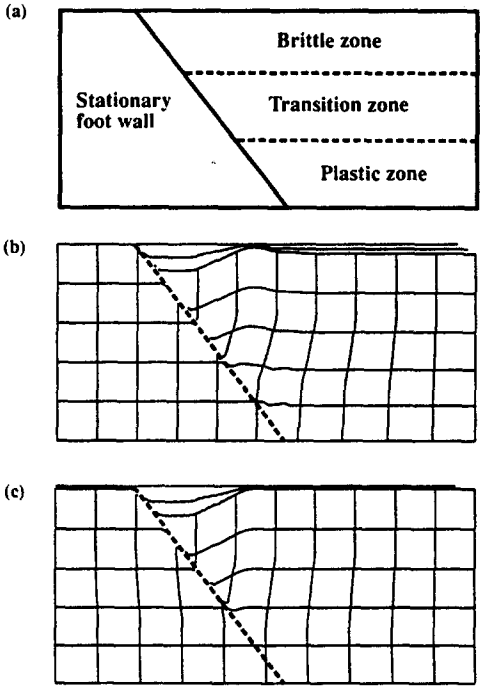

Fig. 3. Computer simulation of extension in a model undergoing brittle deformation at the top and ductile deformation at the bottom. (a) Schematic diagram of the model. The entire right-hand boundary is moving at the same rate and the footwall region remains stationary throughout deformation. (b) The appearance of a grid after 5% extension. Syn-rift layer boundaries have been introduced at the model top after 2.5% and 5% extension. (c) Identical to (b) except the plastic zone extends under the entire width of the model rather than only to the right of the fault.

Note that compaction has not been allowed for in this example although using equation (5) rather than equation (12) would easily allow the following approach to include compaction.

Now, for a finite difference grid with the (i, j)th node at $x = i\Delta x$ and $z = j\Delta z$, equation (12) can be approximated at the point $x = i\Delta x$, $z = (j + \frac{1}{2})\Delta z$, i.e. a point lying half way between two rows of nodes and in a column. After rearrangement this produces

$$v_z(i, j + 1) = v_z(i, j) - \Delta z(\partial v_x/\partial x)_{i,j+1/2}, \quad (13)$$

where

$$(\partial v_x/\partial x)_{i,j+1/2} = [v_x(i + 1, j) - v_x(i - 1, j) + v_x(i + 1, j + 1) - v_x(i - 1, j + 1)]/4\Delta x. \quad (14)$$

Thus, an unknown vertical displacement rate, $v_z(i, j + 1)$, can be calculated from the vertical displacement rate, $v_z(i, j)$, directly below. Note that this is an explicit formulation of the problem not requiring the tridiagonal matrix inversion used by Waltham (1989). Surprisingly, this algorithm produces stable answers and so the Crank–Nicolson (1947) approach is not required.

Another difference between this vertical–horizontal approach and the speed–direction approach is that calculations are performed from bottom to top rather than from hangingwall pin line to fault. Thus, the second bottom row of velocities is calculated using the values in the bottom row, then the third row is calculated from the second and so on up to the top of the model. This has the advantage that a top boundary condition is not required and, instead, boundary conditions are required on both vertical edges of the model (rather than just one). For the problem considered here, these boundary conditions are much easier to specify.

The horizontal velocity field used in Fig. 3 is as follows. In the footwall $v_x = 0.0$ (a small negative value could have been used and this would have produced some footwall uplift). In the brittle zone $v_x = V_{max}$, i.e. constant heave. For the ductile zone, v_x increases linearly from the 'fault' to the right-hand edge where $v_x = V_{max}$. In the transition zone v_x is a weighted average of the brittle value and the ductile value with the weighting linearly dependent on height to give the ductile value at the zone base and the brittle value at the zone top.

The boundary conditions for vertical velocity on the lower and left boundaries are

$$v_z = 0.0 \quad (15)$$

and on the right boundary in the ductile layer

$$v_z = -az, \quad (16)$$

where a is the constant of proportionality used to produce the linearly increasing v_x and z is height above the model base. Note that,because of the inclined fault, a varies with z. In the transition zone the right-hand boundary condition is

$$v_z = V_1 - az/2, \quad (17)$$

where V_1 is the vertical velocity at the top of the ductile

layer, z is height above the base of the transition layer and a is defined as before. Finally, the boundary condition in the brittle layer is

$$v_z = V_2, \tag{18}$$

where V_2 is the vertical velocity at the top of the transition region. Note that the boundary condition in the transition region is intermediate between a constant value, as in the brittle layer, and a linearly varying value, as in the ductile layer.

The boundary condition given by equation (15) produces a bottom boundary which does not move vertically. Thus, the bottom of the model represents a hypothetical depth in the crust which is unaltered by extension. In practice there must be such a depth but there is no reason to suppose, as I have done here, that this depth does not vary with horizontal position and time (Barr 1987a,b).

The remaining boundary conditions ensure smoothly varying behaviour from plastic deformation with a linearly increasing vertical velocity in the bottom third of the model to a constant vertical velocity in the top third of the model.

Points to note about the result, which is shown in Fig. 3(b), are the large subsidence observed near to the fault, at surface, due to a hangingwall rollover and the smaller subsidence in the right half of the model caused by thinning of the ductile layer. Between these two regions of subsidence is a relative high where neither process has much effect. Note also that a zone of distributed shear is generated within the transition region which accommodates the strain between the brittle and plastic parts of the model. This contrasts with previous models in which this strain is accommodated by a detachment at which an instantaneous change from brittle to plastic behaviour occurs (Kusznir *et al.* 1987).

Figure 3(c) is identical to Fig. 3(b) except that the region of plastic deformation extends across the entire width of the model. The boundary conditions used to produce this result are the same as those used to produce Fig. 3(b) except that the left-hand conditions are now the same as those used for the right-hand side in Fig. 3(b). The hangingwall anticline is no longer present and this result, produced by varying the position of the plastic deformation region with respect to the fault, is very similar to that shown by Kusznir *et al.* (1987). In addition, moving the region of plastic deformation under the footwall results in footwall subsidence, although this effect would be modified if isostasy and flexural rigidity were included. The zone of distributed shear now extends under the footwall with an abrupt change in sense from sinistral (footwall) to dextral (hangingwall) at the fault.

DISCUSSION

I have attempted to demonstrate the power and flexibility of the finite difference method for modelling crustal deformation. The technique easily handles problems such as compaction and variation in behaviour with depth and could, in principle, be used to model situations involving compositional inhomogeneities. In addition, by attempting to numerically reproduce the geometries observed in analogue models or natural examples, an insight can be gained into the dynamics involved. No other single technique can handle all of the features modelled in the various sections of this paper, i.e. constant (or any other suitable form) displacement rate on a listric fault; shearing along non-planar surfaces; production of shear and extension strain maps; transition from brittle to ductile behaviour without the use of a detachment surface; and compaction. However, for many applications not requiring these refinements, other simpler techniques should still be preferred and this is particularly true for the inverse problem of predicting fault geometry from bed deformation.

This paper is intended to present general methods rather than specific results. However, several important results have emerged from the examples given. Firstly, to reproduce the broad outlines of the analogue models it is necessary to have the dip of the shearing surfaces decrease with height above the detachment. This implies that strain is more widely distributed at surface than it is at depth and also that bed slip is an important mechanism in hangingwall deformation. Secondly, the failure of the compaction models to produce a hangingwall syncline shows that such a syncline is not a necessary geometric result of compaction and therefore drag in the vicinity of the bounding fault is a more likely mechanism for this frequently observed phenomenon. Finally, the brittle–ductile modelling runs confirm the suggestion of Kusznir *et al.* (1987) that the distribution of pure shear in the lower crust with respect to faulting in the upper crust has an important effect on hangingwall geometry and can, for example, produce a hangingwall anticline from a simple planar fault.

Many refinements to the finite difference modelling of deformation remain to be attempted. For example, isostasy and thermal relaxation are obviously important factors in the situation being modelled in Fig. 3. Can these be included in the finite difference scheme? The effect of compositional inhomogeneities has been touched upon several times in this paper but this work is still in its early stages. The finite difference method could, in principle, also be used to model more complex forms of crustal deformation such as rotating fault blocks above a uniformly extending lower crust. This would require the velocity model to be updated after each increment of extension since the faults themselves would be moving. Unfortunately, it is not clear which boundary conditions should be used for modelling a rotating fault block system and this system has not yet been modelled by the author.

Finally, it should be pointed out that the finite difference technique, as used here, is not a detailed physical model of crustal deformation. Rather, it is a method for visualizing the geometrical consequences of hypotheses such as non-planar shearing surfaces or exponential decrease of porosity with depth.

Acknowledgements—I should like to thank Mike Norton for his helpful comments on this work. I must also thank Ken McClay for his help and for supplying the analogue model result used in this paper. This research was conducted as part of NERC project GR3/6658.

REFERENCES

Barr, D. 1987a. Structural/stratigraphic models for extensional basins of half-graben type. *J. Struct. Geol.* **9**, 491–500.

Barr, D. 1987b. Lithospheric stretching, detached normal faulting and footwall uplift. In: *Continental Extensional Tectonics* (edited by Coward M. P., Dewey, J. F. & Hancock, P. L.). *Spec. Publs geol. Soc. Lond.* **28**, 81–82.

Birkoff, G. 1955. *Hydrodynamics*. Dover publications, New York.

Cloos, E. 1968. Experimental analysis of Gulf Coast fracture patterns. *Bull. Am. Ass. Petrol. Geol.* **52**, 420–444.

Crank, J. & Nicolson, P. 1947. A practical method for numerical evaluation of solutions of partial differential equations of the heat-conduction type. *Proc. Cambridge Phil. Soc.* **43**, 50.

Faugere, E. & Brun, J.-P. 1984. Modelisation experimentale de la distention continentale, Serie II. *C. r. Acad. Sci., Paris* **299**, 365–370.

Jaeger, J. C. 1956. *Elasticity, Fracture and Flow*. Methuen, New York.

Kusznir, N. J., Karner, G. D. & Egan, S. 1987. Geometric, thermal and isostatic consequences of detachments in continental lithosphere extension and basin formation. *Mem. Can. Soc. Petrol. Geol.* **12**, 185–204.

Magara, K. 1978. *Compaction and Fluid Migration Developments in Petroleum Science, Vol.* 9. Elsevier, New York.

McClay, K. R. & Ellis, P. G. 1987. Geometries of extensional fault systems developed in model experiments. *Geology* **15**, 341–344.

Sclater, J. G. & Christie, P. A. F. 1980. Continental Stretching: an explanation of the post-Mid-Cretaceous subsidence of the Central North Sea Basin. *J. geophys. Res.* **85**, 3711–3739.

Steckler, M. S. & Watts, A. B. 1978. Subsidence of the Atlantic margin of New York. *Earth Planet Sci. Lett.* **41**, 1–13.

Verrall, P. 1982. Structural interpretation with application to North Sea problems. Course Notes No. 3. JAPEC.

Waltham, D. 1989. Finite difference modelling of hangingwall deformation. *J. Struct. Geol.* **11**, 433–437.

White, N. J., Jackson, J. A. & McKenzie, D. P. 1986. The relationship between the geometry of normal faults and that of sedimentary layers in their hangingwalls. *J. Struct. Geol.* **8**, 897–910.

Williams, G. & Vann, I. 1987. The geometry of listric normal faults and deformation in their hangingwalls. *J. Struct. Geol.* **9**, 789–795.